

Estimating the contribution of Alfvén waves to the process of heating the quiet solar corona

J. J. González-Avilés^{*} and F. S. Guzmán[†]

Instituto de Física y Matemáticas, Universidad Michoacana de San Nicolás de Hidalgo, Edificio C3, Cd. Universitaria, 58040 Morelia, Michoacán, México.

10 March 2022

ABSTRACT

We solve numerically the ideal MHD equations with an external gravitational field in 2D in order to study the effects of impulsively generated linear and non-linear Alfvén waves into isolated solar arcades and coronal funnels. We analyze the region containing the interface between the photosphere and the corona. The main interest is to study the possibility that Alfvén waves triggers the energy flux transfer toward the quiet solar corona and heat it, including the case that two consecutive waves can occur. We find that in the case of arcades, short or large, the transferred fluxes by Alfvén waves are sufficient to heat the quiet corona only during a small lapse of time and in a certain region. In the case of funnels the threshold is achieved only when the wave is faster than 10 km/s, which is extremely high. We conclude from our analysis, that Alfvén waves, even in the optimistic scenario of having two consecutive Alfvén wave pulses, cannot transport enough energy as to heat the quiet corona.

Key words: MHD - Alfvén waves - Sun: atmosphere - Sun: corona.

1 INTRODUCTION

Recent observations indicate the existence of Alfvén waves (Banerjee et al. 2007), kink waves (Aschwanden et al. 1999; Nakariakov et al. 1999) and torsional Alfvén waves (Jess et al. 2009) in the solar atmosphere. These observations are based on data provided by current space missions, such as Transition Region and Coronal Explorer (TRACE), Solar Dynamics Observatory (SDO), Solar Optical Telescope (SOT), X-ray Telescope (XRT) and Swedish Solar Telescope (SST) (Banerjee et al. 2007; Tomczyk et al. 2007; De Pontieu et al. 2007; Okamoto et al. 2007; Jess et al. 2009). Moreover, it has been observed that the solar atmosphere is permeated by magnetic fields, which are organized in several structures, like small-scale magnetic flux tubes, loops, gravitationally stratified and magnetically confined structures (solar magnetic arcades), weakly curved coronal magnetic flux tubes (coronal funnels), and others, and these structures may support the propagation of different kinds of MHD waves.

We are interested in studying the role that Alfvén waves play in the coronal heating problem, but first we mention the physical mechanisms that have been already proposed to study the problem. Theoretical models of coronal heating mechanisms include Direct Current (DC) and Alternat-

ing Current (AC) models, which characterize the electromechanic coronal response to the photospheric driver that provides the energy source for heating. The DC models involve Ohmic dissipation, magnetic reconnection, current cascading and viscous turbulence (Sturrock & Uchida 1981; Parker 1983; Milano et al. 1999; Gudiksen & Nordlund 2002), and the AC models involve wave heating by Alfvénic resonance (Hollweg 1991), resonant absorption (Davila 1987; Goossens et al. 1992; Ofman & Davila 1994; Erdelyi & Goossens 1994), phase mixing (Parker 1991; De Moortel et al. 1999), current layers (Galsgaard & Nordlund 1996), MHD turbulence (Matthaeus et al. 1999; Dmitruk et al. 2001) and cyclotron resonance (Hollweg 1986; Tu & Marsch 1997). In addition is it considered that some heating could also be produced by compressional waves (acoustic waves) or shocks (Kuperus et al. 1981). Another possible mechanism to heating the solar corona is by magneto-acoustic shock waves generated by chromospheric reconnection (Sturrock 1999; Litvinenko 1999; Sakai et al. 2000; Ryutova et al. 2001).

The theoretical approach is centered in the analysis of numerical simulations modeling the propagation of Alfvén waves in the solar atmosphere, e.g. in (Kudoh & Shibata 1999) numerical simulations have been performed to study torsional Alfvén waves propagation along an open magnetic flux tube in the solar atmosphere. The results suggest that the hot quiet corona, non-thermal broadening of lines, and spicules are all caused by the non-linear Alfvén waves. In

^{*} E-mail: javiles@ifm.umich.mx (JJGA)

[†] E-mail: guzman@ifm.umich.mx (FSG)

(Del Zanna et al. 2005), it has been studied numerically the propagation and evolution of Alfvénic pulses in the solar coronal arcades. The results show a propagation of the initially localized pulses within the solar arcade, due to the variations in the Alfvén speed with height, and therefore an efficient damping of the amplitude of the oscillations. In (Murawski & Musielak 2010) small-amplitude Alfvén waves are modeled by solving the 1D wave equation and it was found that as a result of cut-off frequencies, these waves are not able to propagate freely into the upper regions of the solar atmosphere, undergoing reflection towards lower layers.

On the other hand, in (Ebadi et al. 2012) the dissipation of Alfvén waves due to phase mixing in a stratified environment of solar spicules has been presented. The results show that in the presence of stratification due to gravity, damping takes place. In (Chmielewski et al. 2013), it has been investigated the role of impulsively generated non-linear Alfvén waves in the observed non-thermal broadening of some spectral lines in solar coronal holes. The results were that the non-linear Alfvén waves with amplitude $A_v = 50$ km/s are the most likely candidates for the non-thermal broadening of line profiles in the polar coronal hole. In (Chmielewski et al. 2014a) a 2.5 D numerical model is used to study the propagation and reflection of impulsively generated Alfvén waves within a solar magnetic arcade; the results show that the propagation of Alfvén waves is affected by the spatial dependence of the Alfvén speed, which leads to phase mixing that is stronger for more curved and larger magnetic arcades. In (Chmielewski et al. 2014b) we found a study of the propagation of impulsively generated linear and non-linear Alfvén waves in weakly curved coronal magnetic flux-tubes, or coronal funnels, and it was found that non-linear Alfvén waves may carry enough energy as to heat the coronal funnels and power the solar wind that originates in these funnels.

Within all this rich and well investigated scenario we raise again the question of whether Alfvén waves are capable of transferring enough energy as to heat the quiet corona. Most of the aforementioned studies focused on this question are based on numerical simulations of a single pulse. In this paper we simulate the propagation of two pulses in order to study the possible effects of the interference in the process of energy transfer to the corona.

We study the possible effects of interaction between two impulsively generated Alfvén waves in two configurations of magnetic field: i) solar magnetic arcades, that we assume to be isolated and fixed in time so that they may apply to hold on a quiet corona, and ii) coronal funnels. We are interested in the implications of Alfvén waves in the heat transfer into the corona. We simulate the interaction by launching two pulses separated by a given interval of time between 0 and 50 s, considering that otherwise the two pulses are considered to be independent.

The paper is organized as follows, in section 2 we describe the model of solar atmosphere, the numerical methods we use, and the way we measure the energy flux carried by Alfvén waves. In section 3, we present the results of the numerical simulations for various experiments. Finally, in section 4 we present the conclusions.

2 MODEL AND NUMERICAL METHODS

In this section we describe the equations modeling the plasma, the photosphere-corona interface model, the dimensionless equations solved by our code, the initial conditions of the Alfvén wave pulses and the numerical methods used to solve the evolution equations of the system.

2.1 The system of equations

We consider a gravitationally stratified solar atmosphere, which is described by a plasma obeying the ideal MHD submitted to an external constant gravitational field. We choose to write down these equations in a conservative form, which is optimal for our numerical methods:

$$\frac{\partial \rho}{\partial t} + \nabla \cdot (\rho \mathbf{v}) = 0, \quad (1)$$

$$\frac{\partial (\rho \mathbf{v})}{\partial t} + \nabla \cdot (\rho \mathbf{v} \otimes \mathbf{v} - \frac{\mathbf{B} \otimes \mathbf{B}}{\mu_0} + \mathbf{I} p_t) = \rho \mathbf{g}, \quad (2)$$

$$\frac{\partial E}{\partial t} + \nabla \cdot ((E + p_t) \mathbf{v} - \frac{\mathbf{B}}{\mu_0} (\mathbf{v} \cdot \mathbf{B})) = \rho \mathbf{v} \cdot \mathbf{g}, \quad (3)$$

$$\frac{\partial \mathbf{B}}{\partial t} + \nabla \cdot (\mathbf{v} \otimes \mathbf{B} - \mathbf{B} \otimes \mathbf{v}) = 0, \quad (4)$$

$$\nabla \cdot \mathbf{B} = 0, \quad (5)$$

where ρ is the plasma mass density, $p_t = p + \frac{\mathbf{B}^2}{2\mu_0}$ is the total (thermal + magnetic) pressure, \mathbf{v} represents the plasma velocity field, \mathbf{B} is the magnetic field, μ_0 is the vacuum permeability, \mathbf{I} is the unit matrix and E is the total energy density, that is, the sum of the internal, kinetic, and magnetic energy density

$$E = \frac{p}{\gamma - 1} + \frac{\rho \mathbf{v}^2}{2} + \frac{\mathbf{B}^2}{2\mu_0}. \quad (6)$$

For the fluid we consider an adiabatic index $\gamma = 5/3$. The system of equations (1)-(5) is closed with the ideal gas law

$$p = \frac{k_B}{m} \rho T, \quad (7)$$

where T is the temperature of the plasma, $m = \mu m_H$ is the particle mass, which is specified by a mean molecular weight value of $\mu = 1.24$ for a fully ionized gas (Chmielewski et al. 2014a) and m_H is hydrogen's mass, k_B is Boltzmann's constant. The gravitational source terms on the right hand side of equations (2) and (3) is given by $\mathbf{g} = [0, -g, 0]$ with magnitude $g = 274$ m/s², which holds near the photosphere.

2.2 Dimensionless MHD equations

In order to carry out our numerical calculations we rescale the system (1-5) according to the following conventions. We choose the length scale l_0 , plasma density scale ρ_0 , and magnetic field scale B_0 to fix the unit of time in terms of the Alfvén speed

$$v_0 \equiv v_{A,0} \equiv \frac{B_0}{\sqrt{\mu_0 \rho_0}} \Rightarrow t_0 \equiv \frac{l_0}{v_0}. \quad (8)$$

Table 1. Units used in this paper

Quantity	cgs units
l_0	10^8 cm
v_0	10^8 cm·s ⁻¹
t_0	1 s
ρ_0	10^{-15} gr·cm ⁻³
B_0	14.472 G

Using these basic scale factors l_0 , B_0 , t_0 we define dimensionless independent variables and associated differential operators as follows

$$\bar{l} \equiv \frac{l}{l_0} \Rightarrow \bar{\nabla} \equiv l_0 \nabla, \quad \bar{t} \equiv \frac{t}{t_0} \Rightarrow \frac{\partial}{\partial \bar{t}} \equiv t_0 \frac{\partial}{\partial t}, \quad (9)$$

and consequently the corresponding dimensionless state variables are defined by

$$\begin{aligned} \bar{\rho} &\equiv \frac{\rho}{\rho_0}, & \bar{\mathbf{v}} &\equiv \frac{\mathbf{v}}{v_0}, & \bar{p} &\equiv \frac{p}{\rho_0 v_0^2}, \\ \bar{E} &\equiv \frac{E}{\rho_0 v_0^2}, & \bar{\mathbf{B}} &\equiv \frac{\mathbf{B}}{B_0}, & \bar{\mathbf{g}} &\equiv \mathbf{g} \left(\frac{l_0}{v_0^2} \right). \end{aligned} \quad (10)$$

Finally the dimensionless equations ruling our system are

$$\frac{\partial \bar{\rho}}{\partial \bar{t}} + \bar{\nabla} \cdot (\bar{\rho} \bar{\mathbf{v}}) = 0, \quad (11)$$

$$\frac{\partial (\bar{\rho} \bar{\mathbf{v}})}{\partial \bar{t}} + \bar{\nabla} \cdot (\bar{\rho} \bar{\mathbf{v}} \otimes \bar{\mathbf{v}} - \bar{\mathbf{B}} \otimes \bar{\mathbf{B}} + \mathbf{I} \bar{p}_t) = \bar{\rho} \bar{\mathbf{g}}, \quad (12)$$

$$\frac{\partial \bar{E}}{\partial \bar{t}} + \bar{\nabla} \cdot ((\bar{E} + \bar{p}_t) \bar{\mathbf{v}} - \bar{\mathbf{B}} (\bar{\mathbf{v}} \cdot \bar{\mathbf{B}})) = \bar{\rho} \bar{\mathbf{v}} \cdot \bar{\mathbf{g}}, \quad (13)$$

$$\frac{\partial \bar{\mathbf{B}}}{\partial \bar{t}} + \bar{\nabla} \cdot (\bar{\mathbf{v}} \otimes \bar{\mathbf{B}} - \bar{\mathbf{B}} \otimes \bar{\mathbf{v}}) = \mathbf{0}, \quad (14)$$

$$\bar{\nabla} \cdot \bar{\mathbf{B}} = 0. \quad (15)$$

The dimensionless version of the equation of state (7) is obtained using the definitions of p and ρ

$$p = \frac{k_B}{m} \rho T \Rightarrow \bar{p} = \frac{k_B}{v_0^2 m} \bar{\rho} T, \quad (16)$$

and the dimensionless temperature \bar{T} and equation of state are

$$\bar{T} \equiv T \left(\frac{k_B}{m v_0^2} \right), \quad \bar{p} = \bar{\rho} \bar{T}. \quad (17)$$

In this way, the ideal MHD system (11-15) is attached to the scale length, magnetic field, density and time factors l_0 , B_0 , ρ_0 and t_0 . In our simulations we choose the scale factors in cgs units as specified in Table 1.

2.3 Model of the static solar atmosphere

We specifically center the domain of analysis as one covering part of both the chromosphere and the corona. We consider the atmosphere to be static ($\partial/\partial t = 0$) and study the evolution on a finite xy domain, where the x is a horizontal coordinate and y labels height. All the state variables depend on x and y , but a non-zero component of the velocity field v_z and

a non-trivial magnetic field z -component B_z that vary with x and y are allowed. This kind of model is called a 2.5 dimensional (2.5D) model (Murawski & Musielak 2010; Murawski & Zaqarashvili 2010; Murawski et al. 2011; Woloszkiwicz et al. 2014; Chmielewski et al. 2014a; Chmielewski et al. 2014b).

Given the solar atmosphere is in static equilibrium, it should have a force-free and current-free magnetic field given by the condition

$$\nabla \times \mathbf{B}_e = \mathbf{0} \Rightarrow (\nabla \times \mathbf{B}_e) \times \mathbf{B}_e = \mathbf{0}, \quad (18)$$

where the subscript e stands for equilibrium quantities. The choice of the magnetic field satisfying (18) is general and depends on the physical problem under study. As a result of applying the static equilibrium and the magnetic current-free conditions to equation (2), the pressure gradient is balanced by gravity:

$$-\nabla p_e + \rho_e \mathbf{g} = \mathbf{0}. \quad (19)$$

In addition, following (Murawski & Musielak 2010; Murawski & Zaqarashvili 2010; Murawski et al. 2011; Woloszkiwicz et al. 2014; Chmielewski et al. 2014a; Chmielewski et al. 2014b) we use the ideal gas law (7) and the fact that hydrostatic equilibrium will only hold along the y direction, so that the equilibrium gas pressure takes the form:

$$p_e(y) = p_{ref} \exp \left(- \int_{y_{ref}}^y \frac{dy'}{\Lambda(y')} \right), \quad (20)$$

and the mass density

$$\rho_e(y) = \frac{p_e(y)}{g \Lambda(y)}, \quad (21)$$

where

$$\Lambda(y) = \frac{k_B T_e(y)}{mg}, \quad (22)$$

is the pressure scale-height, and p_{ref} represents the gas pressure at a given reference level, that we choose to be located at $y_{ref} = 10$ Mm, because in the temperature model above, this is the location at which the corona region starts.

2.3.1 Model for isolated solar magnetic arcades

We model an isolated solar magnetic arcade with a magnetic flux-tube model originally developed by (Low 1985) in three dimensions. This model considers a magnetic flux function

$$A(x, y) = \frac{x(y_{ref} - b)^2}{(y - b)^2 - x^2} B_{ref}, \quad (23)$$

where b is a constant that determines the vertical location of a magnetic pole, which is set to $b = -5$ Mm and B_{ref} is the magnetic field strength at y_{ref} . The magnetic field is thus

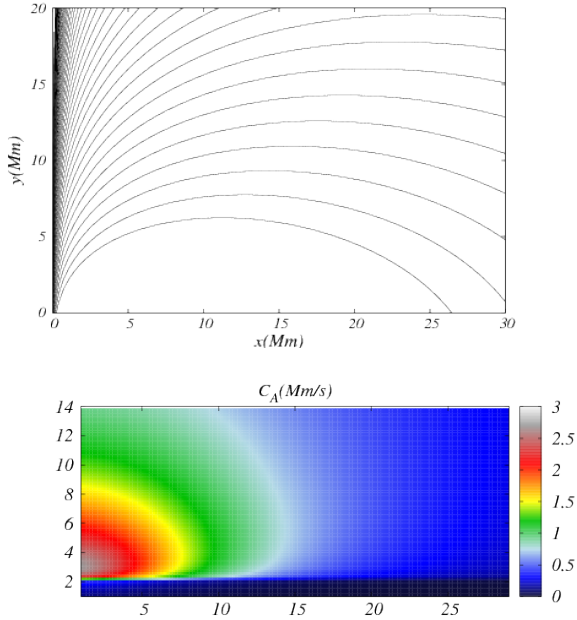


Figure 1. (Top) Magnetic field lines for an open arcade with parameters $B_{ref} = 14.472$ G, $b = -5$ Mm and $y_{ref} = 10$ Mm. (Bottom) The associated Alfvén speed in Mm/s.

$$\mathbf{B}_e(x, y) = \nabla \times (A(x, y)\hat{\mathbf{z}}) = \frac{\partial A(x, y)}{\partial y} \hat{\mathbf{x}} - \frac{\partial A(x, y)}{\partial x} \hat{\mathbf{y}}, \quad (24)$$

where specifically the equilibrium magnetic field components $B_{ex}(x, y)$ and $B_{ey}(x, y)$ are

$$B_{ex}(x, y) = -\frac{2x(y-b)(b-y_{ref})^2}{(x^2 - (b-y)^2)^2} B_{ref}, \quad (25)$$

$$B_{ey}(x, y) = -\frac{(x^2 + (b-y)^2)(b-y_{ref})^2}{(y^2 - 2by - x^2 + b^2)^2} B_{ref}. \quad (26)$$

The value of B_{ref} is chosen such that the Alfvén and sound speeds

$$c_A(x, y) = \sqrt{\frac{B_{ex}^2 + B_{ey}^2}{\mu_0 \rho_e(y)}}, \quad c_s(y) = \sqrt{\frac{\gamma p_e(y)}{\rho_e(y)}}, \quad (27)$$

satisfy the constraint $c_A(0, y_{ref}) = 10c_s(y_{ref})$, because in the solar corona the magnetic pressure is bigger than the fluid pressure. This constraint gives a value of $B_{ref} = 14.472$ G. The magnetic field components resulting from equations (25) and (26) are displayed in Fig. 1 (top). Such magnetic configuration corresponds to an isolated asymmetric magnetic arcade as proposed in (Chmielewski et al. 2014a). As described in equation (27) Alfvén speed depends on x and y , which means that it is non-isotropic as is also shown in Fig. 1 (bottom). This effect will influence the dynamics of the wave.

2.3.2 Model for coronal funnels

Following (Chmielewski et al. 2014b), we assume the magnetic flux function has only a $\hat{\mathbf{z}}$ component and the following expression

$$\mathbf{A}_e(x, y) = \Lambda_B B_{ref} \sin\left(\frac{x}{\Lambda_B}\right) \exp\left(-\frac{y-y_{ref}}{\Lambda_B}\right) \hat{\mathbf{z}}, \quad (28)$$

where B_{ref} is again the magnetic field at the reference level $y_{ref} = 10$ Mm. Unlike (Chmielewski et al. 2014b) we use a sin instead of a cosine in order to be consistent with our convention of coordinates. Here $\Lambda_B = 2L/\pi$ denotes the magnetic scale-height and L is a half of the magnetic arcade width. In this case we want to model weakly expanding coronal funnels, then we fixed $L = 75$ Mm (Chmielewski et al. 2014b). For this choice, the magnetic field lines are weakly curved and represent the open and expanding field lines similar to coronal holes. Finally, the magnetic field reads

$$\mathbf{B}_e(x, y) = \nabla \times (A(x, y)\hat{\mathbf{z}}) = \frac{\partial A(x, y)}{\partial y} \hat{\mathbf{x}} - \frac{\partial A(x, y)}{\partial x} \hat{\mathbf{y}}, \quad (29)$$

and the equilibrium components $B_{ex}(x, y)$ and $B_{ey}(x, y)$ are explicitly

$$B_{ex}(x, y) = -B_{ref} \sin\left(\frac{x}{\Lambda_B}\right) \exp\left(-\frac{y-y_{ref}}{\Lambda_B}\right), \quad (30)$$

$$B_{ey}(x, y) = -B_{ref} \cos\left(\frac{x}{\Lambda_B}\right) \exp\left(-\frac{y-y_{ref}}{\Lambda_B}\right). \quad (31)$$

On the other hand, in this model the Alfvén speed varies only with y because the density does:

$$c_A(y) = \sqrt{\frac{B_{ex}^2 + B_{ey}^2}{\mu_0 \rho_e(y)}} = \frac{B_{ref} e^{-\frac{y-y_{ref}}{\Lambda_B}}}{\sqrt{\mu_0 \rho_e(y)}}, \quad (32)$$

and the equilibrium sound speed is

$$c_s(y) = \sqrt{\frac{\gamma p_e(y)}{\rho_e(y)}}. \quad (33)$$

In addition, B_{ref} must satisfy the condition $c_A(y_{ref}) = 10c_s(y_{ref})$, and once again we set $B_{ref} = 14.472$ G as in the case of magnetic arcades. The resulting magnetic field and Alfvén speed are shown in Fig. 2. Due to the symmetries, unlike the arcade, in this case the Alfvén speed depends only on y .

2.4 Plasma temperature model

The temperature field is assumed to obey the C7 model (Avrett & Loeser 2008). This is a semiempirical model of the chromosphere, with the temperature distribution adjusted to obtain optimum agreement between calculated and observed continuum intensities, line intensities, and line profiles of the SUMER (Curdt et al. 1999) atlas of the extreme ultraviolet spectrum.

We set the temperature profile by interpolation of the data in (Avrett & Loeser 2008) into our numerical domain, and the result is shown in Fig. 3. The main properties of this profile are that T varies nearly three orders of magnitude across the transition between the chromosphere and the corona, ranging from 5000 K at $y = 1.5$ Mm up to 10^6 K at $y = 10$ Mm. For bigger y the temperature profile is assumed to be constant.

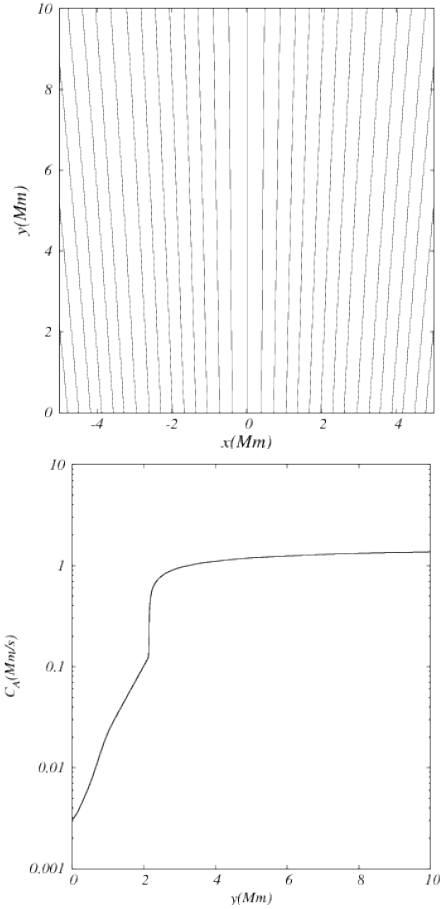


Figure 2. (Top) Magnetic field lines for coronal funnels with parameters $B_{ref} = 14.432$ G, $y_{ref} = 10$ and $\Lambda_B = 150/\pi$ Mm. (Bottom) Alfvén speed as a function of y .

The pressure $p_e(y)$ is integrated numerically using equation (20) and $\rho_e(y)$ is calculated using equation (21). The two profiles are shown in Fig. 4, where the important gradients at the transition region can be seen.

2.5 Initial conditions

Using the previous experience in (Murawski & Musielak 2010; Chmielewski et al. 2013; Wołoszkiewicz et al. 2014; Chmielewski et al. 2014a; Chmielewski et al. 2014b) the Alfvén waves are considered to be perturbations of the z -component of the velocity field v_z with a given profile. In our cases, both for the arcades and the funnels we use the velocity profile in (Chmielewski et al. 2014a) considering a Gaussian profile of the form

$$v_z(x, y, t = 0) = A_v e^{-\frac{(x-x_0)^2}{w_x^2} - \frac{(y-y_0)^2}{w_y^2}}, \quad (34)$$

where A_v is the amplitude of the pulse, (x_0, y_0) is its initial position, w_x and w_y denote the width of the pulse along x and y .

In this paper we consider the interaction between two pulses, one launched at initial time and a second pulse launched after a given delay lapse τ . We study the effects

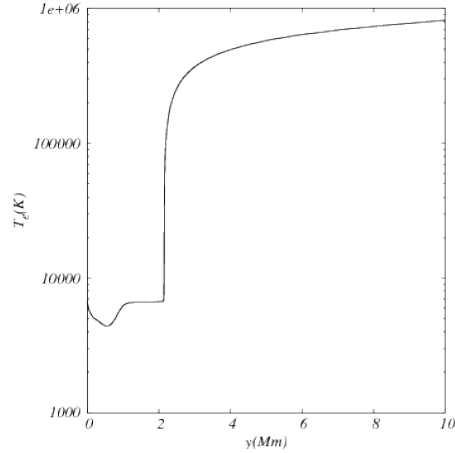


Figure 3. Equilibrium temperature profile for the C7 model interpolated into our numerical domain.

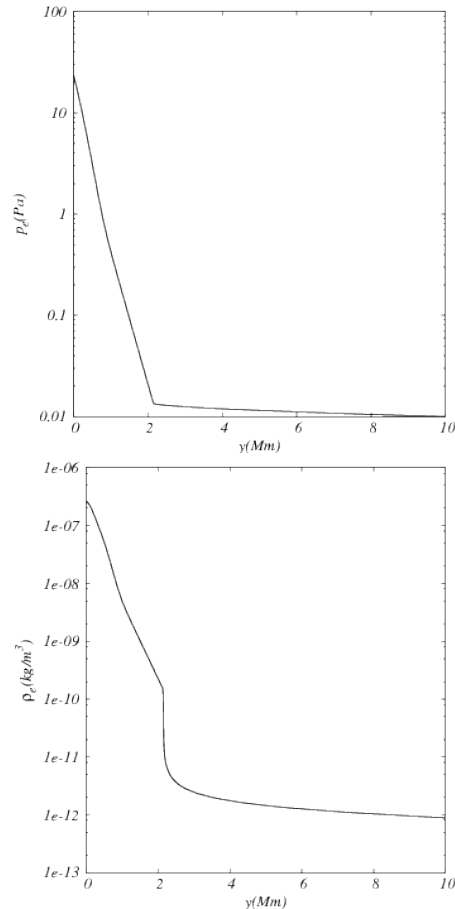


Figure 4. Equilibrium gas pressure (top) and mass density (bottom) for the C7 model.

of the value of the delay lapse on the dispersion of the total energy of the pulses and their capability of transporting energy toward the corona.

2.6 Numerical methods

The equations (11)-(15) are solved numerically using our own numerical code, which is the Newtonian version of CAFE (Lora et al. 2014), that solves the MHD equations on a uniform cell centered mesh in unigrid mode, and has been applied in relativistic scenarios including the accretion on black holes (Lora et al. 2014b; Lora-Clavijo & Guzmán 2013; Cruz-Osorio, et al. 2012; Guzmán & Lora-Clavijo 2011). The integration in time uses the method of lines with a third order Runge-Kutta time integrator (Shu & Osher 1989). The right hand sides of the MHD equations are discretized using a finite volume approximation, together with a High Resolution Shock Capturing method. In all the simulations in this paper, this method uses the HLLE (Harten P. et al. 1983) approximate Riemann solver formula in combination with the second order linear piecewise reconstructor MINMOD.

The numerical evolution of initial data involving Maxwell equations leads to the violation of the divergence free constraint equation (5), developing as a consequence unphysical results like the presence of a magnetic net charge. Among the several methods available to control the growth of the constraint violation (Tóth G. 2000), in our code we use a version of the constrained transport method (CT) proposed in (Evans & Hawley 1988), which is based on the use of the fluxes computed with the conservation scheme itself. This algorithm is known as flux-CT (Balsara 2001), which maintains the constraint small.

We use a 2D domain, and the boundary conditions consist in fixing all the evolution variables at all four boundaries to their equilibrium initial values.

2.7 Alfvén waves and coronal heating

In order to estimate the influence of Alfvén waves as carriers of energy to the solar corona, which eventually would produce the heating of the quiet corona or the acceleration of the solar wind, it is necessary to have flux estimates toward the corona. One way to measure the flux energy carried by Alfvén waves is to consider the Poynting flux given by

$$\mathbf{F}_P = \frac{1}{\mu_0} \mathbf{B} \times (\mathbf{v} \times \mathbf{B}) \quad (35)$$

from which we only take the y -component F_{Py} , that carries energy toward the upper shells. Another usual measurement involves the WKB approximation, which approximates the total flux formula as (Browning 1991; Hollweg 1991; Kudoh & Shibata 1999):

$$F \approx \rho v_z^2 c_A, \quad (36)$$

where ρ is the density, c_A is the local speed of the Alfvén waves and v_z is the Alfvén speed, measured at a particular height. Here we measure both fluxes in order to compare.

A way to estimate whether the Alfvén waves contribute or not to heat the quiet corona is using the threshold in (Withbroe & Noyes 1977), indicating that when the flux exceeds the value $\sim 3 \times 10^5$ erg/s/cm², the contribution to heating is considerable. Usually what is done is that F_{WKB} is measured at a specific point (Kudoh & Shibata 1999; Chmielewski et al. 2014b). Here we measure both fluxes not

at a single point, but in order to have a bigger picture we scan these values in three different points specified for each case.

3 RESULTS OF NUMERICAL SIMULATIONS

We present the results of the energy flux transferred to the corona due to the interaction of two waves evolving on arcades and on funnels. In all cases we estimate the effects of the time elapsed between the two pulses τ . For this we only consider impulsively generated Alfvén waves because their higher amplitude corresponds to a better transport of energy.

3.1 Interaction between two Alfvén waves on a solar magnetic arcade

We set the simulation domain to $[1,29] \times [1,15]$ Mm², covered with 1200×600 cells. We consider large and short arcades, and the length of the arcades depends on the curvature of the magnetic field lines: a) For the large arcades we use $x_0 = 2$ Mm, and the Alfvén waves propagate higher up along longer and more curved magnetic field lines, b) for short arcades we set $x_0 = 3$ Mm, and the inclination of the magnetic field lines is much larger and the magnetic field lines are less curved.

3.1.1 Interaction of two pulses in a large arcade

In this case the amplitude of the initial Gaussian velocity pulse is $A_v = 3$ km/s, the widths are $w_x = 0.2$ Mm, $w_y = 0.1$ Mm and is located initially at $(x_0, y_0) = (2 \text{ Mm}, 1.75 \text{ Mm})$ in (34). We show the results for the particular case in which the second pulse is launched 30 s after the first pulse in Fig. ???. Initially the first pulse decouples into two pulses moving in opposite directions. One pulse propagates downwards very fast, and the second propagates upwards through the chromosphere and transition region to the solar corona, the part of the pulse that propagates upwards reaches the transition region and accelerates due to an increase of the local Alfvén speed as expected for the case of a single pulse in (Chmielewski et al. 2014a). We launch the second pulse at time $t = 30$ s, this pulse clearly affects the propagation of the first pulse. The interaction between the two pulses produces reflections as shown at time $t = 76$ s. Finally by time $t = 106$ s, the waves reach a maximum distance x where they are reflected back to the solar surface. This process shows that phase mixing and reflections grow due to the interaction. Finally, in order to verify our evolution we show at the bottom of Fig. ?? the violation of the magnetic field divergence free constraint.

We perform a series of simulations like this one, for various time lapses between the first and the second pulses τ . We measure F_{Py} and F_{WKB} at three different points and show the measurements in Fig. 6. We plot a line indicating the threshold 3×10^5 erg/s/cm². The results indicate that the Poynting flux measured at the detector located on the left overtakes the threshold during a small lapse of time. The reason is that at this detector the field is more intense. This cannot be observed at other detectors and according to the F_{WKB} the threshold is never achieved.

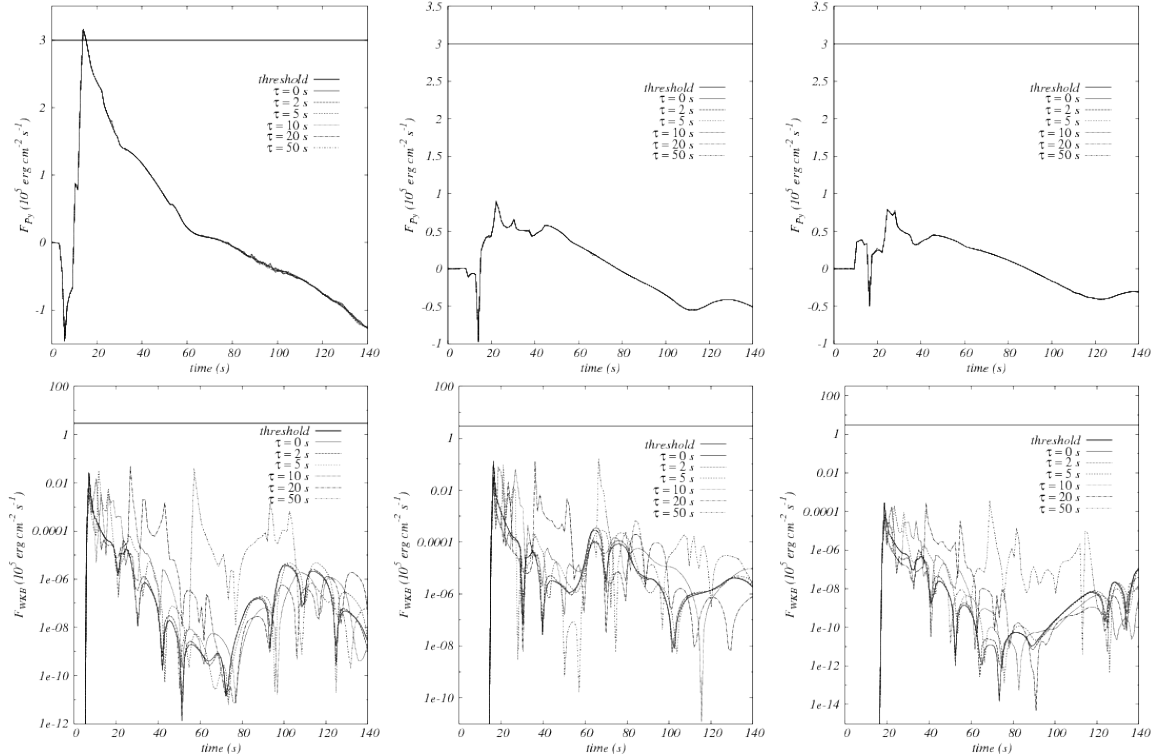


Figure 6. Energy fluxes F_{Py} (top) and F_{WKB} (bottom) for the propagation of two pulses in a large arcade using three detectors (from left to right) located at (7.25, 7) Mm, (14.5, 7) Mm and (14.5, 10) Mm, for $\tau = 0, 2, 5, 10, 20, 50$ s. The continuous line indicates the threshold over which the flux contributes to the coronal heating.

3.1.2 Interaction in a short arcade

In a similar way, we study the propagation of the same velocity Gaussian pulses with $A_v = 3$ km/s, $w_x = 0.2$ Mm, $w_y = 0.1$ Mm and $(x_0, y_0) = (3$ Mm, 1.75 Mm) on a short arcade. In Fig. ?? we show a particular case with $\tau = 20$ s. Again, the initial pulse decouples into two pulses moving in opposite directions. At time $t = 16$ s we only show the part of the pulse that moves upwards without interaction. This pulse is affected by the transition region and phase mixing, which produces the appearance of a fanning with negative amplitude. We launch the second pulse at time $t = 20$ s, which produces interference at time $t = 32$ s. By $t = 40$ s the second pulse suffers the effect of the density decay in the transition region, and the fanning becomes elongated. At time $t = 52$ s the waves reach a maximum distance in w , where they suffer strong reflections. Part of these waves return to the solar surface, so as the energy.

We perform the same experiments as in the previous case for various time lapses between the first and the second pulses. Again we use three detectors to measure F_{Py} and F_{WKB} shown in Fig. 8. Like in the previous case, only the Poynting flux reports values above the threshold in the detector at the left.

3.2 Interaction between two Alfvén waves in a coronal funnel

In this case we set the simulation domain to be $[-5, 5] \times [1, 81]$ Mm², covered with 300×2400 cells. Like in the cases of arcades, we launch two velocity pulses with profile (34)

separated by an interval of time τ on the funnel magnetic field configuration defined in 2.3.2.

3.2.1 Interaction between two Alfvén waves with amplitude $A_v = 10$ km/s

The typical behavior of the pulses is shown in Fig. 9 for $\tau = 10$ s and pulses with parameters $A_v = 10$ km/s, $w_x = w_y = 0.2$ Mm, $(x_0 = 0, y_0 = 1.75)$ Mm. Initially the first pulse decomposes into two propagating waves (Chmielewski et al. 2014b), one pulse that moves upwards and a second pulse that moves downwards. The amplitude of the pulse that moves downwards decays with time and practically disappears. We show the first pulse at time $t = 5$ s, this pulse experiences an acceleration at the transition region due to an increment of the local Alfvén speed c_A . The shape of the pulse becomes ellipsoidal elongated along the vertical direction. Then the second Gaussian pulse appears at time $t = 10$ s. Still by $t = 15$ s the effect of the second pulse is not significant to the shape of the first pulse. However, at that time the pulse that moves upwards suffers another elongation. At later times in the evolution, we can see reflections and phase mixing because of the effect of the transition region in the pulses that move upwards at time $t = 30$ s. The two pulses have already reached the solar corona. At time $t = 60$ s, a signal of v_z with negative amplitude reaches the solar corona, and the pulses that move upwards continue moving vertically.

The fluxes measured at various detectors are shown in Fig. 10. In this case the Poynting flux never reaches the

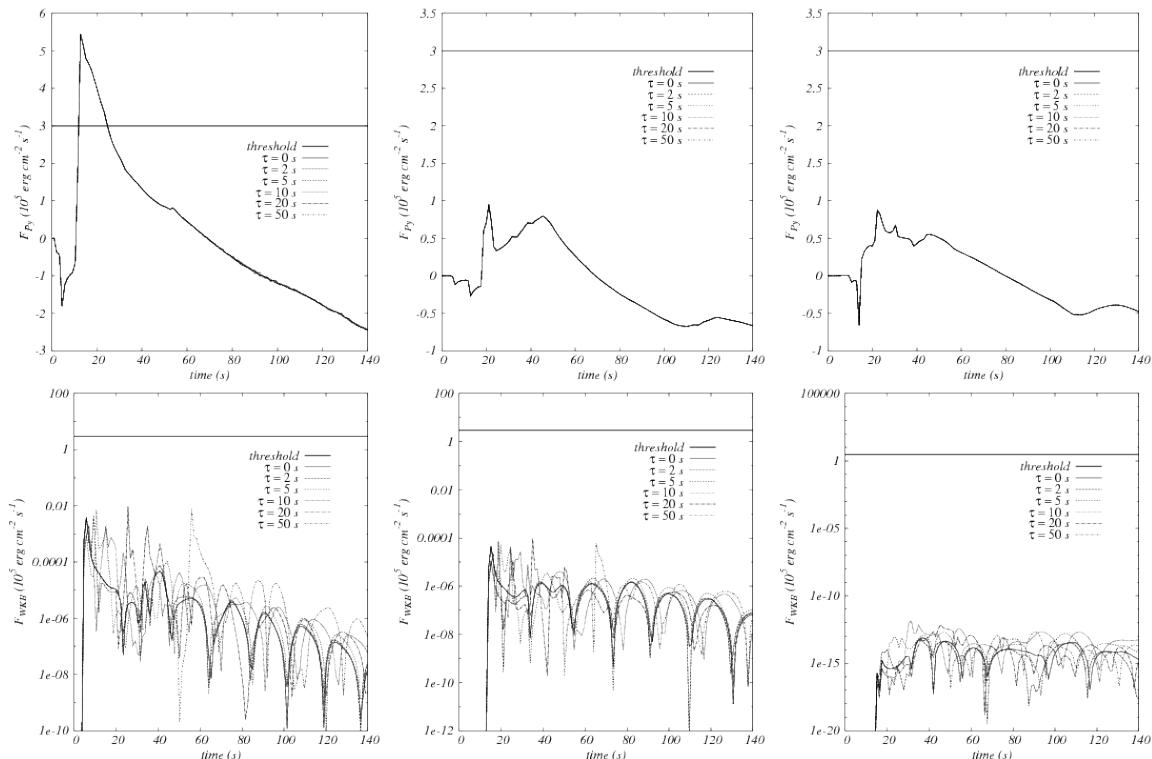


Figure 8. Energy fluxes F_{Py} and F_{WKB} for the propagation of two pulses in a large arcade using three detectors at (7.25, 4.5) Mm, (14.5, 4.5) Mm and (14.5, 7) Mm, for $\tau = 0, 2, 5, 10, 20, 50$ s. Again we show the threshold.

threshold for any of the combination of pulses whereas, unlike the arcade cases, the F_{WKB} flux exceeds the threshold during a small lapse of time for the case $\tau = 5$ s, measured by a detector located along the central vertical line (0,10).

3.2.2 Interaction between two Alfvén waves with amplitude $A_v = 40$ km/s

In order to show the contribution using one of the highest amplitudes found in literature, we prepare a case of an impulsively generated and high amplitude pulse with parameters $A_v = 40$ km/s, $w_x = w_y = 0.2$ Mm, $(x_0 = 0, y_0 = 1.75)$ Mm (Chmielewski et al. 2013; Chmielewski et al. 2014b). We show snapshots of the evolution of the wave in Fig. 11.

In Fig. 12 we show F_{Py} and F_{WKB} at various detectors. We find that the two detectors located at the center of the domain measure fluxes, both F_{Py} and F_{WKB} over the threshold for various values of τ in a generic way.

As mentioned before, this is one of the highest value used to model the propagation of Alfvén waves, however it is not clear from observations that such high speeds have been observed and associated to funnel type of configurations so far. Therefore we have only shown that in the case that such high speeds are observed, they may actually contribute to heating the corona.

4 CONCLUSIONS

We have proposed an optimistic scenario where not only a single Alfvén wave pulse can contribute to heating the quiet

corona, but two possible pulses that may be launched very close in time.

We found that impulsively generated linear Alfvén waves in the solar magnetic arcades, with slow pulses, in large or short arcades, carry enough energy as to heat the solar quiet corona only during a small lapse of time for a very particular combination of pulses, which indicates the threshold is not overtaken for generic combination of pulses.

In the case of the propagation of impulsively generated non-linear Alfvén waves in the coronal funnels, the waves with amplitude $A_v = 10$ km/s do not carry enough energy flux as to heat the solar quiet corona, even if two consecutive pulses are launched. On the other hand, the energy transferred overtakes the threshold by orders of magnitude in the case of waves with an amplitude of $A_v = 40$ km/s, which we cannot be sure that exist but has been mentioned in existing literature.

We conclude from our analysis, that impulsively generated Alfvén waves, even in this optimistic scenario, are unlikely candidates to heat the quiet corona.

ACKNOWLEDGMENTS

We thank Victor De la Luz and Ernesto Aguilar for reading the manuscript and providing important comments. This research is partly supported by grant CIC-UMSNH-4.9.

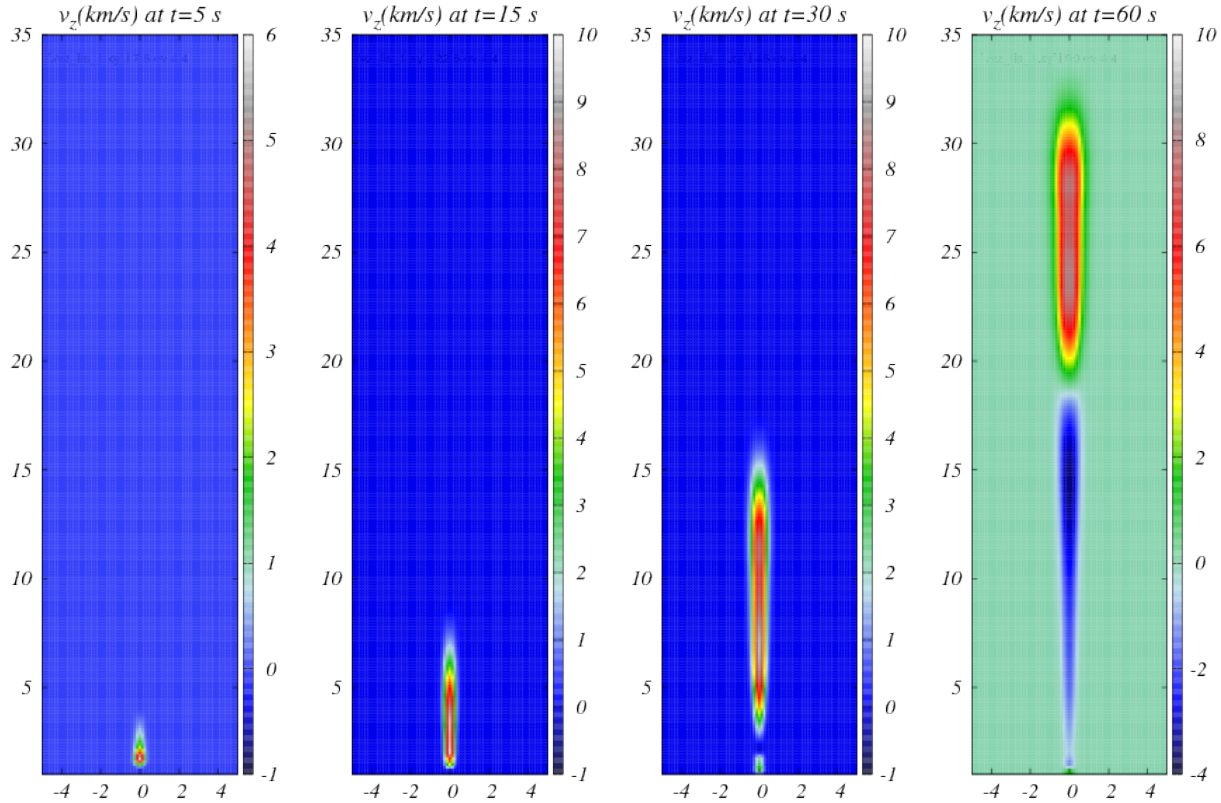


Figure 9. Spatial profiles of the interaction of two non-linear pulses $v_z(x, y, t)$ for $A_v = 10$ km/s, $w_x = w_y = 0.25$ Mm displayed at times $t = 5$ s, $t = 15$ s, $t = 30$ s, $t = 60$ s. In this case $\tau = 10$ s.

REFERENCES

- Aschwanden M. J., Fletcher L., Schrijver C. J., Alexander D., 1999, ApJ, 520, 880
- Avrett E. H., Loeser R., 2008, ApJS, 175, 229
- Balsara, D. S., 2001, ApJS, 132, 83
- Banerjee D., Erdélyi R., Oliver R., O’shea E., 2007, Sol. Phys., 245
- Browning P. K., 1991, Plasma Phys. Control. Fusion, 33, 539
- Chmielewski P., Srivastava A.K., Murawski K., Musielak Z.E., 2013, MNRAS, 428, 40
- Chmielewski P., Murawski K., Musielak Z.E., Srivastava A.K., 2014, ApJ, 793, 43
- Chmielewski P., Srivastava A.K., Murawski K., Musielak Z.E., 2014, Acta Phys. Pol., 125, 1
- Cruz-Osorio, A., Lora-Clavijo, F. D., Guzmán F. S., 2012, MNRAS, 426, 732-738.
- Curd T. W., Heinzel P., Schmidt W., Tarbell T., Uexkull V., Wilken V., 1999, ed. A. Wilson (ESA SP-448; Noordwijk: ESA), 177
- Davila J.M., 1987, ApJ, 317, 514
- Del Zanna L., Schnaekens E., Velli M., 2005, A&A, 431, 1095
- De Moortel I., Hood A.W., Ireland J., et al., 1999, A&A, 346, 641
- De Pontieu B., McIntosh S. W., Carlsson M., Hansteen V. H., Tarbell T. D., Schrijver C. J., Title A. M., Shine R. A., Tsuneta S., Katsukawa Y., Ichimoto K., Suematsu Y., Shimizu T., Nagata S., 2007, Sci, 318, 1574
- Dmitruk P., Milano L.J., Mathhaeus W.H., 2001, ApJ, 548, 482
- Ebadi H., Hosseinpour M., Altafi-Mehrabani H., 2012, Astrophys. Space Sci, 340, 9
- Erdélyi R., Goossens M., 1994, Astrophys. Space Sci, 213, 273
- Evans C.R., Hawley J.F., 1988, ApJ, 332, 659
- Fryxell B., Olson K., Ricker P., Timmes X., Zingale M., Lamb D. Q., Macneice P., Rosner R., Truran J.W., Tufo H., 2000, ApJS, 131, 273
- Galsgaard K., Nordlund A., 1996, J. Geophys. Res., 101, 13, 445
- Goossens M., Hollweg J.V., Sakurai T., 1992, SP, 138, 233
- Gudiksen B.V., Nordlund A., 2002, ApJ, 572, L113
- Guzmán F. S., Lora-Clavijo, F. D. 2011, MNRAS, 415, 225-234. Ibid. 2011, MNRAS, 416, 3083-3088.
- Harten P., Lax P. D., Van Leer B., 1983, SIAM review 25, 35
- Hollweg J. V., 1986, J. Geophys. R., 91, 4111
- Hollweg J. V., 1991, Mechanisms of Chromospheric and Coronal Heating ed P Ulmschneider, E R Priest and R Rosner (Berlin:Springer) p 300
- Jess D.B., Mathioudakis M., Erdlyi R., Crockett P.J., Keenan F.P., Christian D.J., 2009, Sci, 323, 1582
- Kudoh T., Shibata K., 1999, ApJ, 514, 493
- Kuperus, M., Ionson J.A., Spicer D., 1981, ARAA, 19, 7

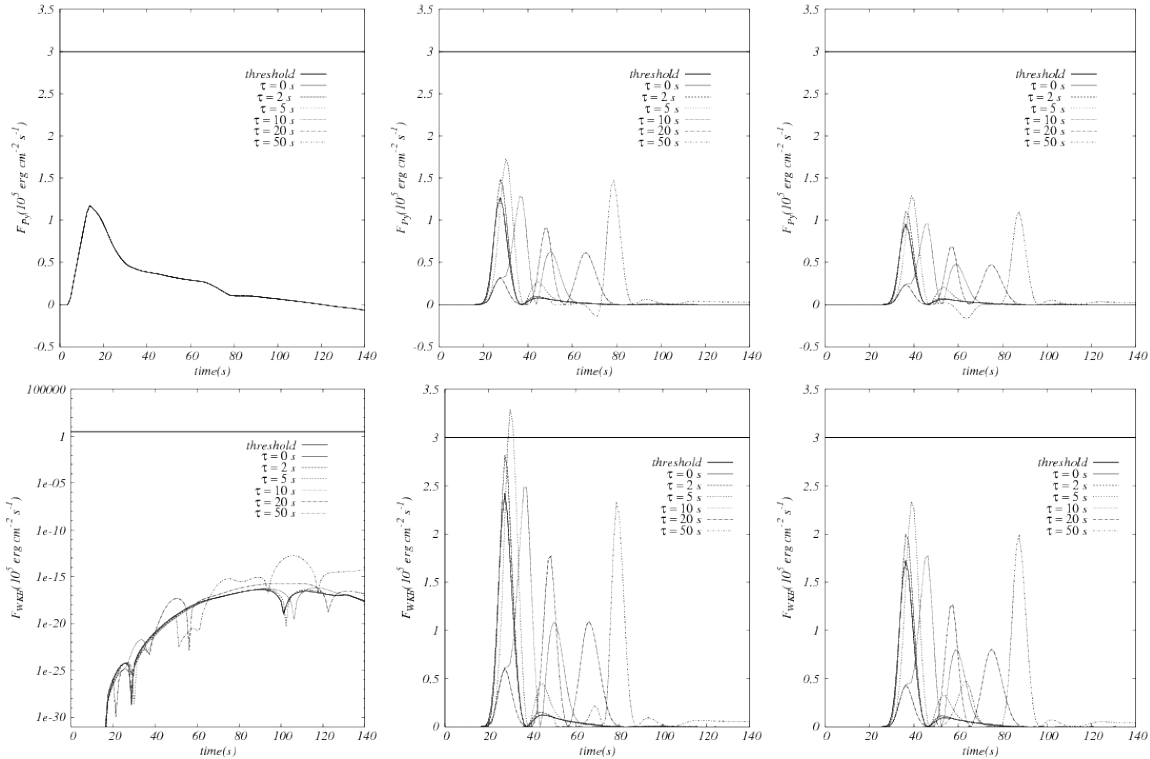


Figure 10. Energy fluxes F_{Py} and F_{WKB} for the propagation of two pulses in a coronal funnel using three detectors at $(-2.5, 10)$ Mm, $(0, 10)$ Mm and $(0, 15)$ Mm, for $\tau = 0, 2, 5, 10, 20, 50$ s. The threshold is achieved only for a particular combination $\tau = 5$ s, however this is not a generic case.

Lee D., 2013, *J. Comp. Phys.*, 243, 269

Lee D., Deane A.E., 2009, *J. Comp. Phys.*, 228, 952

Litvinenko Y.E., 1999, *ApJ*, 515, 435

Lora-Clavijo, F. D., Guzmán F. S., 2013, *MNRAS*, 429, 3144-3154.

Lora-Clavijo F. D., Cruz-Osorio A., Guzmán F. S., 2014, arXiv:1408.5846

Lora-Clavijo F. D., Gracia-Linares, M., Guzmán F. S., 2014, *MNRAS*, 443, 2242-2251.

Low B.C., 1985, *ApJ*, 293, 31

Matthaeus W.H., Zank G.P., Smith C.W., Oughton S., 1999, *Phys. Rev. Lett.*, 823, 3444

Mignone A., Bodo G., Massaglia S., Matsakos T., Tesileanu O., Zanni C., Ferrari A., 2007, *ApJS*, 170, 228

Milano L.J., Dmitruk P., Mandrini C.H., et al., 1999, *ApJ*, 521, 889

Murawski K., Musielak Z. E., 2010, *A&A*, 518, A37

Murawski K., Srivastava A. K., Zaqarashvili T. V., 2011, *A&A*, 535, A58

Murawski K., Zaqarashvili T. V., 2010, *A&A*, 519, A8

Murawski K., Srivastava A. K., Musielak Z. E., 2014, *ApJ*, 788, 1

Nakariakov V. M., Ofman L., Deluca E. E., Roberts B., Davila J. M. 1999, *Sci*, 285, 862

Ofman L., Davila J.M., 1994, *GRL*, 21/20, 2259

Okamoto T.J., Tsuneta S., Berger T.E., Ichimoto K., Katsukawa Y., Lites B.W., Nagata S., Shibata K., Shimizu T., Shine R.A., Suematsu Y., Shimizu T., Nagata S., 2007, *Sci*, 318, 1574

Parker E.N., 1983, *ApJ*, 264, 642

Parker E.N., 1991, *ApJ*, 376, 355

Priest E. R., 1982, in *Solar Magnetohydrodynamics* (Dordrecht:Reidel)

Ryutova M., Habbal S., Woo R., et al., 2001, *Sol. Phys.*, 200, 213

Sakai J.I., Kawata T., Hoshida K., et al., 2000, *ApJ*, 537, 1063

Shu C. W., Osher S. J., 1989, *J. Comp. Phys.*, 83, 32

Srivastava A. K., Dwivedi B. N., 2007, *JA&A*, 28, 1

Srivastava A. K., Konkol P., Murawski K., Dwivedi B.N., Mohan A., 2014, *Sol. Phys.*, 10, 1007

Stone J.M., Gardiner T.A., Teuben P., Hawley J.F., Simon J.B., 2008, *ApJS*, 178, 137

Sturrock P.A., Uchida Y., 1981, *ApJ*, 246, 331

Sturrock P.A., 1999, *ApJ*, 521, 451

Tomczyk S., McIntosh S. W., Keil S. L., Judge P. G., Schad T., Seely D. H., Edmondson J., 2007, *Sci*, 317, 1192

Tóth G., 2000, *J. Comp. Phys.*, 161, 605

Tu C.Y., Marsch E., 1997, *Sol. Phys.*, 171, 363

Tu C. Y., Zhou C., Marsch E., Xia L. D., Zhao L., Wang J. X., Wilhelm K., 2005, *Sci*, 308, 519

Vernazza J.E., Avrett E.H., Loeser R., 1981, *ApJS*, 45, 635

Withbroe G. L., Noyes R. W., 1977, *ARA&A*, 15, 363

Wolozkiewicz P., Murawski K., Musielak Z. E., Mignone A., 2014, *Control and Cybernetics*, 43, 2

This paper has been typeset from a $\text{\TeX}/\text{\LaTeX}$ file prepared by the author.

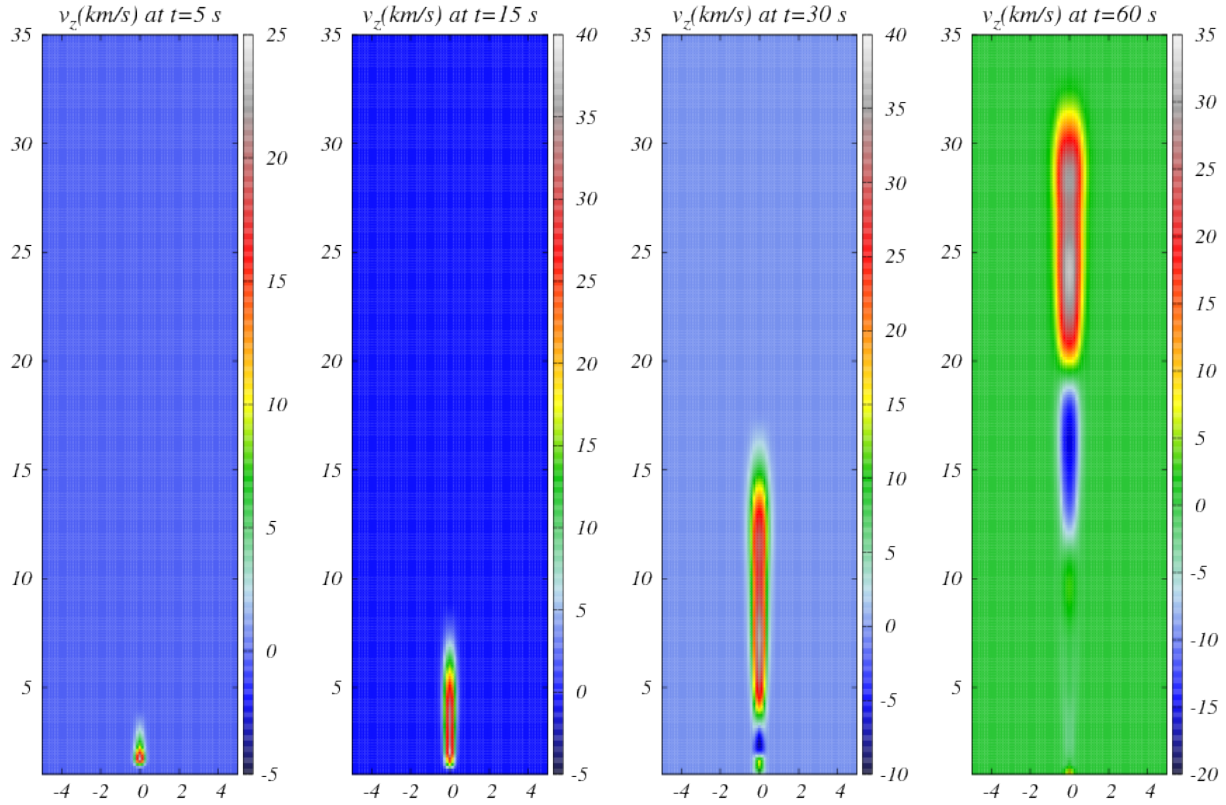


Figure 11. Spatial profile of the interaction of two non-linear pulses $v_z(x, y, t)$ for $A_v = 40$ km/s, $w_x = w_y = 0.2$ Mm displayed at times $t = 5$ s, $t = 15$ s, $t = 30$ s, $t = 60$ s. In this case $\tau = 10$ s.

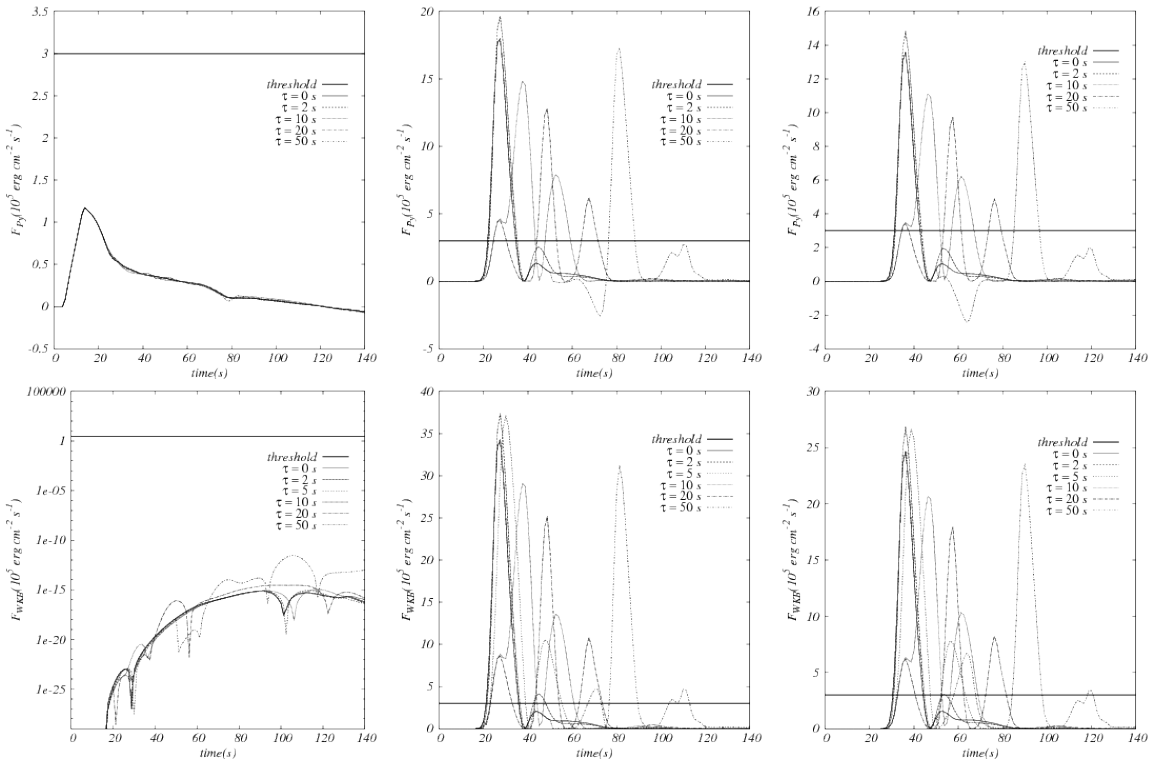


Figure 12. Energy fluxes $F_{P\gamma}$ and F_{WKB} for the propagation of two pulses in a coronal funnel using three detectors at $(-2.5, 10)$ Mm, $(0, 10)$ Mm and $(0, 15)$ Mm, for $\tau = 0, 2, 5, 10, 20, 50$ s. The threshold is overtaken in a systematic way for all the values of τ used.